Antiferromagnetic ground state with pair-checkerboard order in FeSe

Hai-Yuan Cao, Shiyou Chen, Hongjun Xiang, and Xin-Gao Gong

Key Laboratory for Computational Physical Sciences (MOE), State Key Laboratory of Surface Physics,
Collaborative Innovation Center of Advanced Microstructure,
and Department of Physics, Fudan University, Shanghai 200433, China

A monolayer FeSe thin film grown on $SrTiO_3(001)$ (STO) shows the sign of $T_c > 77$ K, which is higher than the T_c record of 56 K for bulk FeAs-based superconductors. However, little is known about the magnetic ground state of FeSe, which should be closely related to its unusual superconductivity. Previous studies presume the collinear stripe antiferromagnetic (AFM) state as the ground state of FeSe, the same as that in FeAs superconductors. Here we find a magnetic order named the "pair-checkerboard AFM" as the magnetic ground state of tetragonal FeSe. The pair-checkerboard order results from the interplay between the nearest-, next-nearest, and unnegligible next-next-nearest neighbor magnetic exchange couplings of Fe atoms. The monolayer FeSe in pair-checkerboard order shows an unexpected insulating behavior with a Dirac-cone-like band structure related to the specific orbital order of the d_{xz} and d_{yz} characters of Fe atoms, which could explain the recently observed insulator-superconductor transition. The present results cast insights on the magnetic ordering in FeSe monolayer and its derived superconductors.

The high-temperature (high-T_c) superconductivity discovered in iron-based superconductors [1–3] breaks the conventional knowledge that magnetic atoms such as Fe should not contribute to superconductivity. This indicates that the magnetism plays an important role in the mechanism of high-T_c superconductivity in iron-based superconductors [4]. Although the electronic properties for different families of iron-based superconductors can be somehow different [5], they all are believed to share common features of antiferromagnetic (AFM) ordered parent compounds [6].

While the magnetism contributing to high-T_c superconductivity has attracted wide attention [7], the magnetic ground states for the parent compounds of iron-based superconductors remain unclear. Recently, the sign of over 77 K unconventional high-T_c superconductivity [8–11] has been observed in monolayer FeSe grown on a $SrTiO_3(001)$ (STO) substrate [12–17], which is much higher than the highest T_c recorded in the intensively studied FeAs systems [18,19]. For FeAs-based materials, the collinear AFM (or the stripe AFM) has been verified as the ground state for the parent compounds by neutron scattering [7]. However, the ground state for the compound based on FeSe is still waiting to be clarified. Previous theoretical studies presumed that FeSe has the same ground state as FeAs-based materials [20–24]. From previous experimental results, the electronic properties of FeSe-based materials have been shown to be much different from those of FeAs-based materials [25], especially for those in monolayer FeSe on a STO substrate [8–17]. A recent angle-resolved photoemission spectroscopy (ARPES) experiment observed an insulator-superconductor transition via doping in a monolayer FeSe grown on a STO substrate [17], which indicates that the ground state of monolayer FeSe could be insulating. In addition, in the recently discovered molecular-intercalated iron-selenide $Li_x(ND_2)_y(ND_3)_{1-y}Fe_2Se_2$ [26], neutron-inelastic-scattering measurements found that the magnetic scattering in momentum space is unusually closer to the wave vector $(\pi, \frac{\pi}{2})$ [27], which means that in FeSe there could be an unexpected magnetic order other than collinear AFM.

Therefore, unveiling the ground-state properties of FeSe would be crucial in understanding the mechanism of novel high-T_c superconductivity.

Here, based on first-principles calculations, we find a magnetic order, named the pair-checkerboard AFM, which is quite different from previously proposed magnetic order in iron-based compounds, to be the magnetic ground state [Fig. 1(a)] for tetragonal FeSe [28]. The underlying physics of this magnetic order could be effectively described by a Heisenberg model including the nearest-, next-nearest, and next-next-nearest neighbor superexchange interactions mediated by Se-$4p$ orbitals. This ground state is metallic in bulk FeSe, while it has a Dirac-cone-like band structure with a nonzero band gap induced by a spin-orbit interaction in monolayer FeSe, where an interlayer interaction between the FeSe layers is absent. The pair-checkerboard AFM would also induce a 2×1 reconstruction in FeSe due to the different distances of the Se atoms to the Fe plane. Furthermore, we confirm that this pair-checkerboard AFM not only exists in tetragonal FeSe, but also in its derived compounds, such as the recently synthesized bulk $LiFeO_2Fe_2Se_2$ [29]. This shows that the magnetic ground state of FeSe is different from that of FeAs-based materials, which could well explain several intriguing experimental observations.

In this Rapid Communication, we performed an extensive study of the electronic and magnetic properties of FeSe based on first-principles simulations. We employed the plane-wave basis set and the projected augmented wave method [30,31] which is implemented in the VASP code [32,33] to calculate the electronic and magnetic properties. We adopted the generalized gradient approximation (GGA) with the Perdew-Burke-Ernzerhof (PBE) formula [34] for the exchange-correlation functional. A plane-wave cutoff energy of 450 eV and a Monkhorst-Pack mesh of 16×8 k points [35] for monolayer FeSe and $18 \times 9 \times 9$ k points for bulk FeSe with 0.1 eV Gaussian smearing were used in magnetic unit cell calculations. A supercell of 16 Fe atoms was used to calculate the magnetic exchange coupling parameters. A vacuum layer

TABLE I. Energy difference ΔE (reference to the energy of the nonmagnetic state) and magnetic moments M_{Fe} of the bulk and monolayer FeSe with different magnetic orders.

	ΔE_{bulk} (meV/f.u.)	M_{bulk} (μ_B)	ΔE_{mono} (meV/f.u.)	M_{mono} (μ_B)
Nonmagnetic order	0	0	0	0
Collinear AFM	−69	1.9	−87	1.9
Checkerboard AFM	−41	1.7	−62	1.7
Bicollinear AFM	−21	2.2	−37	2.2
Pair-checkerboard AFM	−84	2.0	−99	2.0

more than 20 Å thick was used in the calculation for monolayer FeSe to ensure decoupling between neighboring FeSe layers. For structural relaxation, all the atoms were allowed to relax until the atomic forces were smaller than 0.01 eV/Å. The density of states calculations were performed based on the tetrahedral method [36] with a much denser k grid of 24×12 and $24 \times 12 \times 12$ for the magnetic unit cell of monolayer FeSe and bulk FeSe, respectively. Both the lattice constant and the atomic positions were fully optimized.

Our results show that the magnetic ground state of FeSe should be the pair-checkerboard AFM with the magnetic wave vector $\mathbf{Q} = (\pi, \frac{\pi}{2})$, rather than the collinear AFM, which it was assumed to be. We have calculated the relative energy of various magnetic orders, including the nonmagnetic state, the checkerboard AFM order (or the Néel AFM), the bicollinear AFM order, the collinear AFM order, and the pair-checkerboard AFM. Table I lists the energies and the magnetic moments for both the bulk FeSe and monolayer FeSe. One can clearly see that the energy of the pair-checkerboard AFM is lower than that of the collinear AFM order by 15 and 12 meV/f.u. for the bulk FeSe and monolayer FeSe, respectively, while the magnetic moments in the bulk FeSe and monolayer FeSe are quite similar. In fact, we have confirmed that the pair-checkerboard AFM is stable in monolayer FeSe on the STO substrate, and is also stable in the tetragonal phase of FeSe. The breaking of the C_4 symmetry is found in the pair-checkerboard AFM order as well as in the collinear AFM,

which could be caused by the ferro-orbital order [37] or the magnetic fluctuation of Fe atoms in FeSe [38].

The pair-checkerboard AFM is different from the collinear AFM order in that each spin of an Fe atom has one neighbor spin aligned ferromagnetically while the other three neighbor spins are all aligned antiferromagnetically [Fig. 1(a)]. More interestingly, we find an apparent difference between the charge-density distribution of the pair-checkerboard AFM and the collinear AFM [Figs. 1(b) and 1(c)]. Both Fe and Se atoms in the pair-checkerboard AFM order have a unique orbital order which does not appear in other AFM orders. The Se atoms could be divided into two groups [labeled Se1 and Se2 in Fig. 1(b)] with different distances between the Se atoms and the Fe plane (z_{Se}). The z_{Se} for Se1 is 1.48 Å and that for Se2 is 1.46 Å, which can be regarded as a 2×1 reconstruction in FeSe.

The electronic band structure and the projected partial density of states (PDOS) of bulk and monolayer FeSe with the pair-checkerboard AFM state is shown in Figs. 2 and 3, respectively. For bulk FeSe, the band structure shows that there are two electron pockets located around the Γ point and along the X'-Γ line, and one hole pocket centered around the Z point. From the projected PDOS, we find the band crossing the Fermi level mainly coming from the d_{xz} and d_{yz} orbitals, which is caused by the interlayer interaction between adjacent FeSe layers in bulk FeSe. The PDOS of Fe atoms near the Fermi level looks similar for both bulk FeSe and monolayer FeSe, which means that the intralayer interaction in FeSe layers could probably dominate the major physics related to the superconductivity in FeSe.

The tetragonal FeSe with pair-checkerboard AFM order has a feature of an exotic Dirac-cone-like band structure, as shown in Figs. 2(a) and 2(b), respectively. If including the spin-orbit coupling (SOC), monolayer FeSe with the pair-checkerboard AFM becomes insulating with a band gap around 27 meV, while that with other magnetic orders is all metallic. It is worth noting that both the valence band maximum (VBM) and the conduction band minimum (CBM) of the band structure are located around the k point $(0.2, 0.0, 0.0)$ in the Γ-X boundary of the first magnetic Brillouin zone.
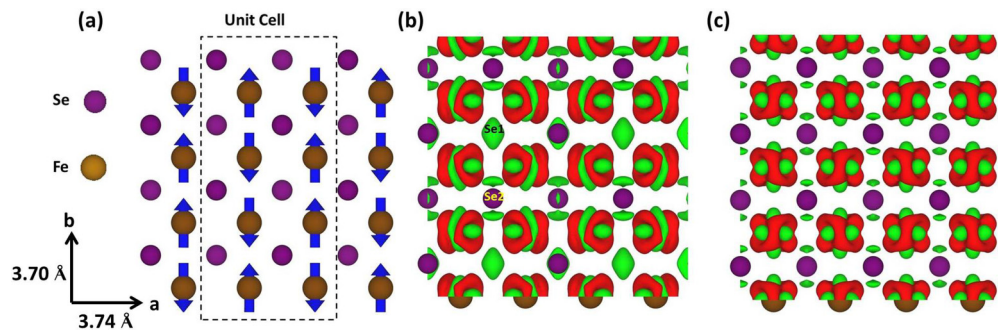

FIG. 1. (Color online) (a) Schematic top view of the pair-checkerboard AFM in an FeSe layer. Each spin of the Fe atom has only one neighbor spin aligned ferromagnetically while the other neighbor spins are all aligned antiferromagnetically. The rectangle enclosed by the dashed lines denotes the magnetic unit cell. The optimized lattice constants for the orthorhombic phase are shown in the figure. (b) The charge-density difference between the pair-checkerboard AFM and the nonmagnetic state. (c) The charge-density difference between the collinear AFM and the nonmagnetic state. The isosurface depicted by the red and green colors represents the lost and gained charge density compared to the nonmagnetic state. Se atoms in the pair-checkerboard AFM order show orbital orders which are labeled Se1 (blue) and Se2 (yellow), respectively.
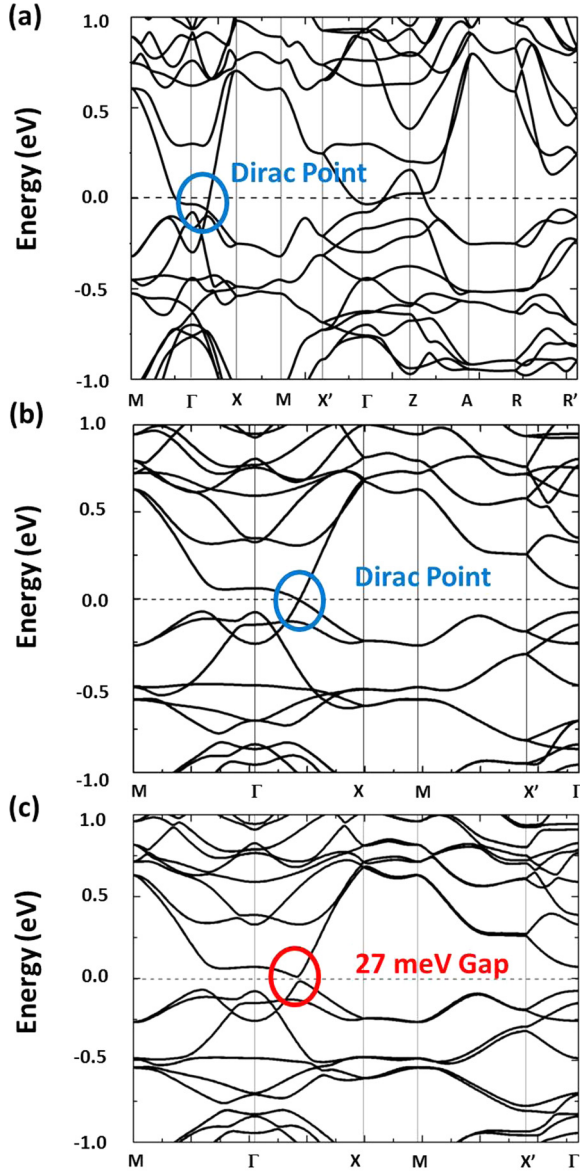
FIG. 2. (Color online) (a) Electronic band structure of bulk FeSe with the pair-checkerboard AFM. (b), (c) Electronic band structure of monolayer FeSe in the pair-checkerboard AFM order without or with spin-orbit coupling. The Dirac point appears in the bulk FeSe and monolayer FeSe (highlighted), while including SOC would open (highlighted) a 27 meV indirect band gap in monolayer FeSe. The Fermi level is denoted by the dashed line.

The Dirac-cone-like band structure relates to a specific orbital order of the d_{xz} and d_{yz} characters of Fe atoms, which can be seen from the decomposed band structure near the Fermi level (see Supplemental Material Fig. S2 [39]). The spin-majority d orbitals of Fe atoms are almost all filled, while the density of states (DOS) near the Fermi level is mostly contributed by the spin-minority d orbitals of the Fe atoms. For the spin-minority part of the Fe atoms, $d_{x^2-y^2}$, d_{z^2}, and d_{xz} orbitals are mostly filled while d_{yz} and d_{xy} orbitals are slightly filled [Fig. 3(b)]. The two bands that cross over the Fermi level are mainly composed of spin-minority d_{xz} and d_{yz} characters of the Fe atoms, respectively. If they are without spin-orbit coupling, d_{xz} and d_{yz} belong to different symmetry

groups which allow them to cross without hybridization at the Fermi level. Then, turning on the spin-orbit coupling could lead to a mixing between d_{xz} and d_{yz} orbitals, resulting in a gap opening. The charge density at the VBM is mainly composed of d_{xz} hybridized with d_{xy} and d_{z^2} of the Fe atoms, while that at the CBM is mainly composed of d_{yz} hybridized with d_{xy} [Fig. 3(b)]. The charge-density distribution at the VBM and CBM is in agreement with the ferro-orbital order of d_{xz} and d_{yz} orbitals [37]. The emerging Dirac-cone-like band structure in the pair-checkerboard AFM should be directly related to the magnetic ground state in monolayer FeSe, which means that the orbital order and the magnetic order are strongly coupled together.

To further describe the origin of the magnetic order in FeSe quantitatively, we propose a frustrated Heisenberg model with the nearest-, next-nearest, and next-next-nearest neighbor couplings J_1, J_2, and J_3 [23],

$$H = J_1 \sum_{\langle ij \rangle} \vec{S}_i \cdot \vec{S}_j + J_2 \sum_{\langle\langle ij \rangle\rangle} \vec{S}_i \cdot \vec{S}_j + J_3 \sum_{\langle\langle\langle ij \rangle\rangle\rangle} \vec{S}_i \cdot \vec{S}_j, \quad (1)$$

where $\langle ij \rangle$, $\langle\langle ij \rangle\rangle$, and $\langle\langle\langle ij \rangle\rangle\rangle$ denote the summation over the nearest-, next-nearest, and next-next-nearest neighbors, respectively. The present model includes the next-next-nearest magnetic coupling J_3, and this is crucial to correctly describe the magnetic ground state in FeSe. According to the band structure of FeSe, we believe that our Heisenberg model could capture the substantial physics in the magnetic properties. Mapping from the calculated energy of different magnetic orders, we find that for bulk FeSe, $J_1 = 47$ meV/S^2, $J_2 = 27$ meV/S^2, and $J_3 = 7$ meV/S^2, while for monolayer FeSe, $J_1 = 44$ meV/S^2, $J_2 = 25$ meV/S^2, and $J_3 = 6$ meV/S^2.

It is known that when $J_2 > \frac{J_1}{2}$, the collinear AFM rather than the checkerboard AFM would be the magnetic ground state in a J_1-J_2 AFM square lattice. If further including $J_3 > \frac{J_2}{2}$ in the model, the magnetic ground state would turn out to be the bicollinear AFM [23]. In our calculation for FeSe, we find that $J_2 > \frac{J_1}{2}$ and $\frac{J_2}{2} > J_3 > \frac{2J_2-J_1}{2}$, and under this condition the magnetic order we propose turns out to be the magnetic ground state in FeSe.

LiFeO$_2$Fe$_2$Se$_2$, an FeSe-based superconductor with $T_c \sim$ 43 K and neutral LiFeO$_2$ anti-PbO-type spacer layers intercalated between FeSe layers, was recently synthesized by the hydrothermal method [29]. The relative energy difference between various magnetic orders in LiFeO$_2$Fe$_2$Se$_2$ is similar to that in FeSe (see Supplemental Material Table S1 [39]). The calculation shows that the pair-checkerboard AFM is not only the magnetic ground state for LiFeO$_2$Fe$_2$Se$_2$, but its relative stability to other magnetic states is even more robust compared to that of monolayer FeSe. This reveals that the pair-checkerboard AFM could be the universal magnetic ground state for the FeSe layer and its derived undoped materials. In addition, we also find that the Dirac-cone-like band structure may still be kept in bulk LiFeO$_2$Fe$_2$Se$_2$.

In previous experiments, a direct observation of the pair-checkerboard AFM order in bulk tetragonal FeSe was lacking. This could probably be attributed to the absence of a high-quality FeSe sample. The extra Fe atoms in the FeSe samples could suppress the stability of the pair-checkerboard AFM order (see Supplemental Material Fig. S4 [39]). Although the pair-checkerboard AFM order still needs to be observed
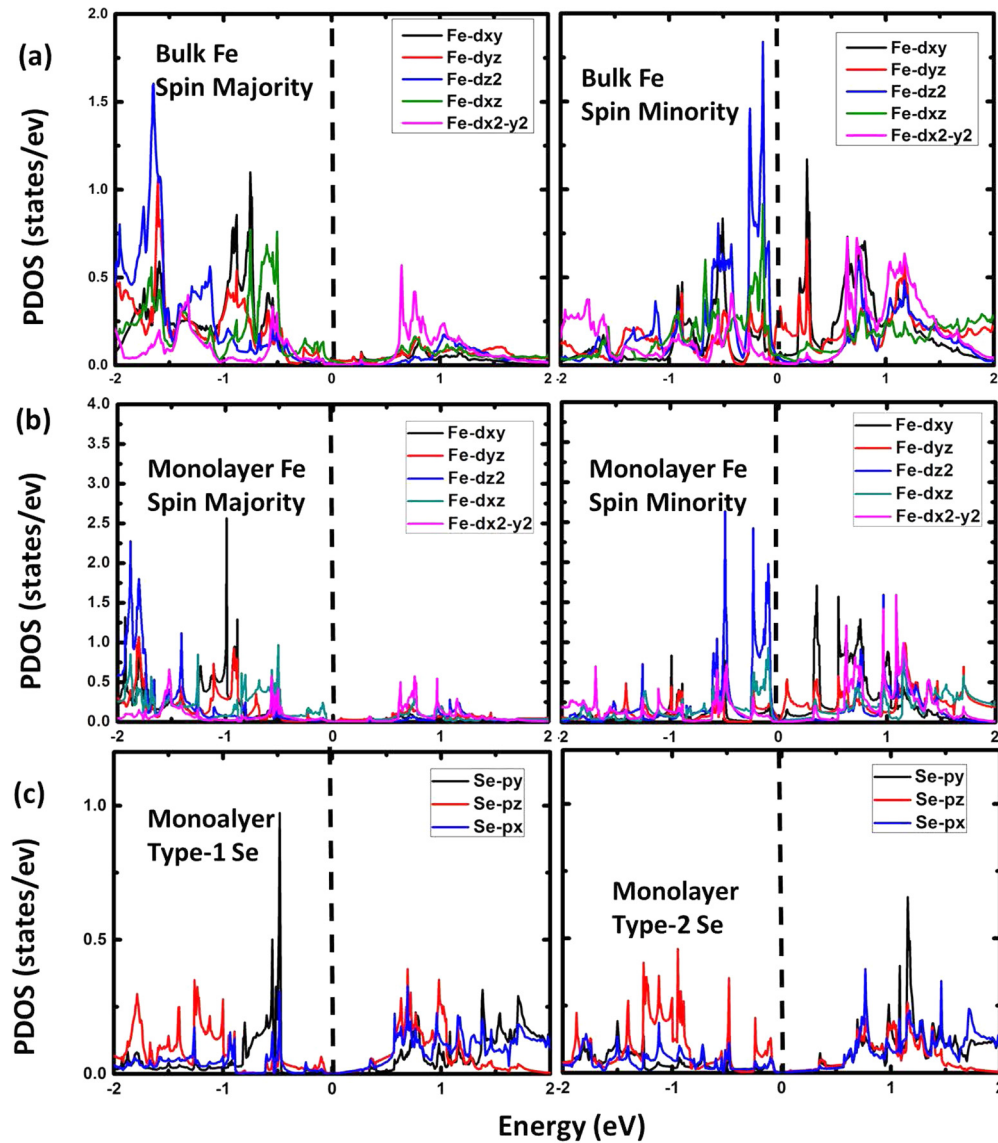
FIG. 3. (Color online) Projected orbital-resolved partial density of states of (a) the spin-majority part and spin-minority part of the Fe atom in bulk FeSe, (b) spin-majority part and spin-minority part of the Fe atom in monolayer FeSe, and (c) type-1 Se atom and type-2 Se atom [defined in (b)], respectively. The d orbitals of Fe atoms diminish to 0 at the Fermi level in monolayer FeSe, while the spin-minority parts of the d_{xz} and d_{yz} orbitals cross the Fermi level in bulk FeSe. The position of the Fermi level is denoted by the dashed lines.

directly, there were several experimental evidences indicating the existence of this magnetic order. First, the 27 meV band gap we predicted in an FeSe monolayer with the pair-checkerboard AFM order is quite close to the ARPES experimentally observed insulating gap of 20–25 meV [17], while that with other magnetic orders all remains metallic. Another scanning tunnel microscopy (STM) experiment observed that a 2×1 reconstruction would occur in monolayer FeSe on the STO substrate [40], which is also coincident with two types of Se atoms with different height z_{Se} in pair-checkerboard AFM. Very recently, electric transport measurements observed Dirac-cone-like ultrafast carriers in a single crystal FeSe superconductor [41], which could also be interpreted as originating from our proposed pair-checkerboard AFM order induced Dirac-cone-like band structure.

In summary, the present studies reveal that FeSe does not share the same collinear AFM magnetic ground state with FeAs-based materials. The magnetic ground state of FeSe is the pair-checkerboard AFM, which is metallic in bulk FeSe and insulating with a 27 meV band gap in monolayer FeSe, and completely different from the magnetic states found in other iron-based superconductors. Such a magnetic order is found to be robust against tensile strain up to a few percent and also robust against electron doping to a certain level (see Supplemental Material Fig. S4 [39]). The properties of the predicted gapped insulating ground state are in good agreement with recent experimental observations [17,40,41]. The pair-checkerboard AFM order in FeSe sheds light on the understanding of high-T_c superconductivity in the FeSe monolayer on the oxide substrates and FeSe-layer-derived superconductors. The pair-checkerboard AFM order we predict calls for more direct experiments to investigate the magnetic properties in high-quality FeSe samples.

[1] Y. Kamihara, T. Watanabe, M. Hirano, and H. Hosono, J. Am. Chem. Soc. **130**, 3296 (2008).

[2] M. Rotter, M. Tegel, and D. Johrendt, Phys. Rev. Lett. **101**, 107006 (2008).

[3] F.-C. Hsu, J.-Y. Luo, K.-W. Yeh, T.-K. Chen, T.-W. Huang, P. M. Wu, Y.-C. Lee, Y.-L. Huang, Y.-Y. Chu, D.-C. Yan, and M.-K. Wu, Proc. Natl. Acad. Sci. USA **105**, 14262 (2008).

[4] D. J. Scalapino, Rev. Mod. Phys. **84**, 1383 (2012).

[5] D. C. Johnston, Adv. Phys. **59**, 803 (2010).

[6] Y. J. Uemura, Nat. Mater. **8**, 253 (2009).

[7] P. Dai, J. Hu, and E. Dagotto, Nat. Phys. **8**, 709 (2012).

[8] Q.-Y. Wang, Z. Li, W.-H. Zhang, Z.-C. Zhang, J.-S. Zhang, W. Li, H. Ding, Y.-B. Ou, P. Deng, K. Chang, J. Wen, C.-L. Song, K. He, J.-F. Jia, S.-H. Ji, Y.-Y. Wang, L.-L. Wang, X. Chen, X.-C. Ma, and Q.-K. Xue, Chin. Phys. Lett. **29**, 037402 (2013).

[9] L. Z. Deng, B. Lv, Z. Wu, Y. Y. Xue, W. H. Zhang, F. S. Li, L. L. Wang, X. C. Ma, Q. K. Xue, and C. W. Chu, Phys. Rev. B **90**, 214513 (2014).

[10] R. Peng, H. C. Xu, S. Y. Tan, H. Y. Cao, M. Xia, X. P. Shen, Z. C. Huang, C. H. P. Wen, Q. Song, T. Zhang, B. P. Xie, X. G. Gong, and D. L. Feng, Nat. Commun. **5**, 5044 (2014).

[11] J.-F. Ge, Z.-L. Liu, C. Liu, C.-L. Gao, D. Qian, Q.-K. Xue, Y. Liu, and J.-F. Jia, Nat. Mater., doi:10.1038/nmat4153 (2014).

[12] D. Liu, W. Zhang, D. Mou, J. He, Y.-B. Ou, Q.-Y. Wang, Z. Li, L. Wang, L. Zhao, S. He, Y. Peng, X. Liu, C. Chen, L. Yu, G. Liu, X. Dong, J. Zhang, C. Chen, Z. Xu, J. Hu, X. Chen, X. Ma, Q. K. Xue, and X. J. Zhou, Nat. Commun. **3**, 931 (2012).

[13] S. L. He, J. F. He, W. H. Zhang, L. Zhao, D. F. Liu, X. Liu, D. X. Mou, Y. B. Ou, Q. Y. Wang, Z. Li, L. L. Wang, Y. Y. Peng, Y. Liu, C. Y. Chen, L. Yu, G. D. Liu, X. L. Dong, J. Zhang, C. T. Chen, Z. Y. Xu, X. Chen, X. C. Ma, Q. K. Xue, and X. J. Zhou, Nat. Mater. **12**, 605 (2013).

[14] S. Tan, Y. Zhang, M. Xia, Z. R. Ye, F. Chen, X. Xie, R. Peng, D. F. Xu, Q. Fan, H. C. Xu, J. Jiang, T. Zhang, X. C. Lai, T. Xiang, J. P. Hu, B. P. Xie, and D. L. Feng, Nat. Mater. **12**, 634 (2013).

[15] W.-H. Zhang, Y. Sun, J.-S. Zhang, F.-S. Li, M.-H. Guo, Y.-F. Zhao, H.-M. Zhang, J.-P. Peng, Y. Xing, H.-C. Wang, T. Fujita, A. Hirata, Z. Li, H. Ding, C.-J. Tang, M. Wang, Q.-Y. Wang, K. He, S.-H. Ji, X. Chen *et al.*, Chin. Phys. Lett. **31**, 1 (2014).

[16] X. Liu, D. F. Liu, W. H. Zhang, J. F. He, L. Zhao, S. L. He, D. X. Mou, F. S. Li, C. J. Tang, Z. Li, L. L. Wang, Y. Y. Peng, Y. Liu, C. Y. Chen, L. Yu, G. D. Liu, X. L. Dong, J. Zhang, C. T. Chen, Z. Y. Xu *et al.*, Nat. Commun. **5**, 5047 (2014).

[17] J. He, X. Liu, W. Zhang, L. Zhao, D. Liu, S. He, D. Mou, F. Li, C. Tang, Z. Li, L. Wang, Y. Peng, Y. Liu, C. Chen, L. Yu, G. Liu, X. Dong, J. Zhang, C. Chen, Z. Xu, X. Chen, X. Ma, Q. K. Xue, and X. J. Zhou, Proc. Natl. Acad. Sci. USA **111**, 18501 (2014).

[18] Z.-A. Ren, W. Lu, J. Yang, W. Yi, X.-L. Shen, Z.-C. Li, G.-C. Che, X.-L. Dong, L.-L. Sun, F. Zhou, and Z.-X. Zhao, Chin. Phys. Lett. **25**, 2215 (2008).

[19] C. Wang, L. Li, S. Chi, Z. Zhu, Z. Ren, Y. Li, Y. Wang, X. Lin, Y. Luo, S. Jiang, X. Xu, G. Cao, and Z. Xu, Europhys. Lett. **83**, 67006 (2008).

[20] A. Subedi, L. J. Zhang, D. J. Singh, and M. H. Du, Phys. Rev. B **78**, 134514 (2008).

[21] T. Bazhirov and M. L. Cohen, J. Phys.: Condens. Matter **25**, 105506 (2013).

[22] K. Liu, Z.-Y. Lu, and T. Xiang, Phys. Rev. B **85**, 235123 (2012).

[23] F. Ma, W. Ji, J. Hu, Z.-Y. Lu, and T. Xiang, Phys. Rev. Lett **102**, 177003 (2009).

[24] H.-Y. Cao, S. Tan, H. Xiang, D. L. Feng, and X.-G. Gong, Phys. Rev. B **89**, 014501 (2014).

[25] E. Dagotto, Rev. Mod. Phys. **85**, 849 (2013).

[26] M. Burrard-Lucas, D. G. Free, S. J. Sedlmaier, J. D. Wright, S. J. Cassidy, Y. Hara, A. J. Corkett, T. Lancaster, P. J. Baker, S. J. Blundell, and S. J. Clarke, Nat. Mater. **12**, 15 (2013).

[27] A. E. Taylor, S. J. Sedlmaier, S. J. Cassidy, E. A. Goremychkin, R. A. Ewings, T. G. Perring, S. J. Clarke, and A. T. Boothroyd, Phys. Rev. B **87**, 220508(R) (2013).

[28] D. P. Landau and K. Binder, Phys. Rev. B **31**, 5946 (1985).

[29] X. F. Lu, N. Z. Wang, G. H. Zhang, X. G. Luo, Z. M. Ma, B. Lei, F. Q. Huang, and X. H. Chen, Phys. Rev. B **89**, 020507(R) (2014).

[30] P. E. Blöchl, Phys. Rev. B **50**, 17953 (1994).

[31] G. Kresse and D. Joubert, Phys. Rev. B **59**, 1758 (1999).

[32] G. Kresse and J. Furthmüller, Comput. Mater. Sci. **6**, 15 (1996).

[33] G. Kresse and J. Furthmüller, Phys. Rev. B **54**, 11169 (1996).

[34] J. P. Perdew, K. Burke, and M. Ernzerhof, Phys. Rev. Lett. **77**, 3865 (1996).

[35] H. J. Monkhorst and J. D. Pack, Phys. Rev. B **13**, 5188 (1976).

[36] P. E. Blöchl, O. Jepsen, and O. K. Andersen, Phys. Rev. B **49**, 16223 (1994).

[37] C.-C. Lee, W.-G. Yin, and W. Ku, Phys. Rev. Lett. **103**, 267001 (2009).

[38] I. I. Mazin, Physica C **469**, 614 (2009).

[39] See Supplemental Material at http://link.aps.org/supplemental/10.1103/PhysRevB.91.020504 for the Brillouin zone used in the calculation of the band structure, the orbital decomposed band structure, the charge-density plot at the Dirac point for monolayer FeSe, the relative energy of bulk $LiFeO_2Fe_2Se_2$ with different magnetic order, and the stability of pair-checkerboard AFM order against strain and charge doping.

[40] J. Bang, Z. Li, Y. Y. Sun, A. Samanta, Y. Y. Zhang, W. Zhang, L. Wang, X. Chen, X. Ma, Q.-K. Xue, and S. B. Zhang, Phys. Rev. B **87**, 220503(R) (2013).

[41] K. K. Huynh, Y. Tanabe, T. Urata, H. Oguro, S. Heguri, K. Watanabe, and K. Tanigaki, Phys. Rev. B **90**, 144516 (2014).